TOLERANCES FOR ECHO-SEEDING IN THE FLASH ORS SECTION

Kirsten Hacker, TU Dortmund, Holger Schlarb, DESY Hamburg

Abstract

This note describes the tolerances for echo-seeding experiments in the FLASH Optical Replica Synthesizer (ORS) section in spring of 2012. A particular case of echo-seeding at the 19th harmonic in the ORS section at a beam energy of 1.15 GeV was simulated and optimized with 1-D particle tracking and an equation that predicts the phase dependence of echo-seeding done with low-dispersion chicanes. The output of this simulation was used to start simulations of a 14 nm FEL beam in the sFLASH undulators. The requirements of an HGHG experiment using the 3rd harmonic of the 14 nm FEL beam were also explored. Tolerances of beam chirps, synchronization, magnet field errors, synchrotron radiation, and microbunching noise were investigated.

INTRODUCTION

Echo-Enabled Harmonic Generation (EEHG), also known as echo-seeding, is a technique which was proposed in 2008 [1,2,3,4] that calls for the co-propagation of an electron bunch and laser pulse through an -undulator, chicane, undulator, chicane- series (Fig. 1). Through interaction with a seed laser, the electron beam develops an energy modulation in a first undulator which is then over-compressed in a first chicane, creating a charge density modulation in longitudinal phase space consisting of thin diagonal stripes of high-charge density separated by low-charge density stripes. The electron bunch is then modulated again in a second undulator and compressed in a second chicane, resulting in vertical stripes of charge with a period consistent with a harmonic of the seed laser wavelength (Fig. 2). Since the Liouville's theorem is not violated, the overcompression process causes an effective reduction of the slice energy spread, making high bunching factors possible.

EEHG schemes have recently been proposed for several seeded FELs [5,6,7] and proof-of-principle experiments at two facilities have been able to generate low-harmonics of the seed laser wavelength [8,9]. These EEHG schemes all call for a large, 1-10 mm, R_{56} in the first chicane and when one sees that the FLASH ORS section chicanes can only achieve a maximum R_{56} of ~130 μm, one is initially inclined to reject the possibility of doing EEHG with this section, even though an ideal laser is available and the – undulator, chicane, undulator, chicane – layout looks appropriate.

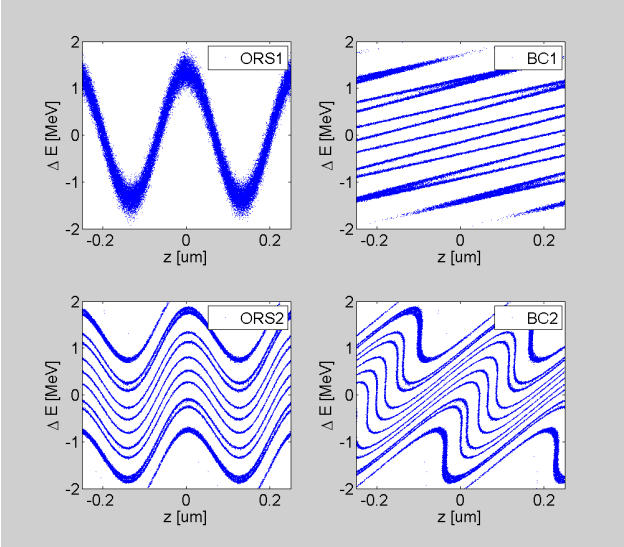

Figure 2: ORS-section EEHG scheme. The beam energy is modulated by a laser in the first undulator (ORS1), over-compressed in the first chicane (BC1), modulated again in the second undulator (ORS2), and compressed in the second chicane (BC2). Parameters for this particular 19th harmonic scheme were, E_0 = 1.15GeV, σ_E = 150 keV, λ = 270 nm, ΔE_1 = 1.3 MeV, ΔE_1 = 0.67 MeV, $R_{56}^{(1)}$ = 550 μm, $R_{56}^{(2)}$ = 90 μm.

However, by increasing the length of the correctors, one can achieve a maximum R_{56} of 700 μm in the first chicane of the ORS section and while this is somewhat small compared to other proposed schemes [5,6,7], we will demonstrate that a wide range of harmonics could be pursued with EEHG in this section.

One option for ORS EEHG is to generate the 19th harmonic of 270 nm so that the beam can lase with 14 nm in the sFLASH undulators. With a beam energy of 1.15 GeV, there is then the possibility to use the 14 nm radiation in an HGHG scheme to produce seeded 4.7 nm in the SASE undulators.

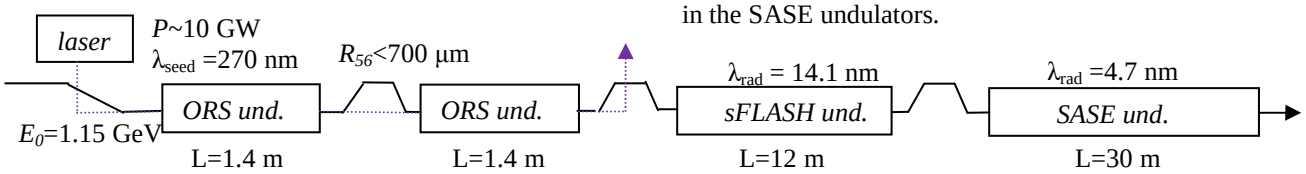

Figure 1: The FLASH I ORS section is located directly prior to the sFLASH undulators. The sFLASH undulators are followed by a small chicane and the "SASE" undulators. Using EEHG to seed the sFLASH undulator section with 14 nm could enable an HGHG scheme to seed the SASE undulator section with 4.7 nm. The laser, diagnostics, chicanes, and undulators are already commissioned. A laser transport line and a small modification to the first chicane are all that is needed to complete this scheme.

The optimization of this scheme was pursued with 1-D tracking code and an equation that predicts the phase sensitivity of higher harmonics produced through EEHG with low-dispersion chicanes. The effects of coherent and incoherent synchrotron radiation (CSR and ISR) on the high peak currents have also been studied along with the effects of electron beam chirp and laser pulse chirp. These results were compared to the simulations that have been done for the FLASH II EEHG scheme [7].

To make this experiment happen in 2012, a new, 12 meter long, evacuated laser transport line will be constructed during the last 3 months of 2011. The first ORS chicane will also be upgraded with longer corrector magnets. A description of the diagnostic, seeding and slicing experiments these upgrades will enable is given in the accompanying TESLA-FEL report [10], the difficulties associated with parasitic operation are explored in TESLA-FEL report [11], and the EEHG hardware and experimental setup are detailed in TESLA-FEL report [12]. This report will focus on simulations and tolerances for echo-seeding experiments at FLASH.

THEORY AND SIMULATION

Eq. 5 of [1] gives the absolute value of the bunching factor for EEHG harmonic numbers n and m,

$$\left|b_{n,m}\right| = \left| J_m(-A_2 B_2 (Km+n)) J_n(-A_1 (B_1 n + B_2 (Km+n)) e^{-\frac{1}{2}(nB_1+B_2(Km+n))^2} \right|$$

where $A=\Delta E/\sigma_E$ and $B=2\pi R_{56}\sigma_E/(E_0\lambda)$ are constants for the first and second undulator and chicane sections. They are written in terms of energy modulation, ΔE, energy spread, σ_E, dispersion, R_{56}, energy, E_0, and seed wavelength, λ. K is the ratio between the seed wavelengths in the first and second undulator. Because we are using one laser wavelength to seed both undulators, K=1.

When designing an EEHG experiment, there is a tendency [5,6,7,8] to search for working points using Eq. 6 of [1], the bunching factor for an EEHG scheme with n = -1,

$$b_{n=-1,m} = \left| J_m(A_2 B_2 (m-1)) J_1(B_1 - B_2 (m-1)) e^{-\frac{1}{2}(B_1 - B_2(m-1))^2} \right|$$

This gives an accurate prediction of the performance of an EEHG scheme if $\Delta z/\lambda >> 1$.

When the R_{56} in the first chicane is small, however, the scheme becomes sensitive to the phase of the laser in the first undulator relative to the phase of the laser in the second undulator. While, strictly speaking, this phase does not change when one uses a single laser, because the phase of the seed laser is written onto the electron beam in the first undulator, changes in this phase are effectively caused by the changes in the arrival-time of the electron bunch after the first chicane. Because the energy stability of the FLASH linac is $\sim 5\cdot 10^{-4}$, we should expect phase changes over a full-cycle of the 270 nm seed wavelength and because the sub millimeter R_{56} of the chicane produces diagonal charge density streaks instead of completely horizontal streaks, one cannot neglect the influence of the laser phase in low-R_{56} EEHG theory.

For this low-R_{56} regime one must remove the absolute value brackets from Eq. 5 of [2] and multiply by $e^{im\varphi}$, where φ is the phase between the electron bunch and the laser pulse in the second undulator. One can then take the sum over all harmonic numbers, n, and phases, φ, in order to predict the phase sensitivity of the bunching factor for harmonic numbers $a=n+m$, such that,

$$b_a(\varphi) = \sum_n e^{in\varphi} b_{n,m} \,. \qquad (1)$$

This is similar to Eq. 14 of [2]. The phase in Eq. (1) refers to the difference between the arrival-time of the electron bunch relative to the arrival-time of the laser pulse after the first chicane. To verify the accuracy of the prediction from Eq. (1), 1-D particle tracking was done with Matlab.

Analytic 1-D and 3-D estimates of the influence of CSR and ISR on the EEHG process were made. Because the characteristic overtaking length from equation 24 in [13] is much smaller than the length of the bends in the chicanes, a steady-state CSR calculation can be used as an approximation. It is, however, verified that the CSR effect is highly over-estimated in 1-D, due to the transverse smearing effect that occurs in 3-D beams due to the R_{53} and R_{54} terms.

The laser power levels (P) required for the various energy modulations, ΔE, used throughout the document are calculated with the formula [2]

$$P = P_0 \left(\frac{E_0 \Delta E \sigma / K_u L_u E_e}{(J_0(K^2/(4+2K^2)) - J_1(K^2/(4+2K^2)))} \right)^2$$

where K_u is the ORS undulator parameter, L_u is the ORS undulator length, E_e is the rest energy of an electron, and the electron beam energy is E_0. For a 740 μm (FWHM) laser beam waist placed in between the two undulators, 320 μm (rms) as the average laser beam diameter (σ) in each undulator. In accordance with the recommendations from [2], this laser beam diameter is >3 times larger than the expected 100 μm (rms) electron beam diameter.

OPTIMIZATION

While particle tracking takes a cumbersome amount of computing time in a search for an optimal working point, with the analytic solution given by the sum over the phase dependent bunching factors (Eq. 1), one can quickly scan over wide parameter ranges and see features that were not apparent with the n=-1 bunching equation. In Fig. 3, scans over a range of R_{56}s are shown for three different laser power combinations and for constants: a = 19, E_0 = 1.15 GeV, σ_E = 150 keV, λ = 270 nm. The islands of high

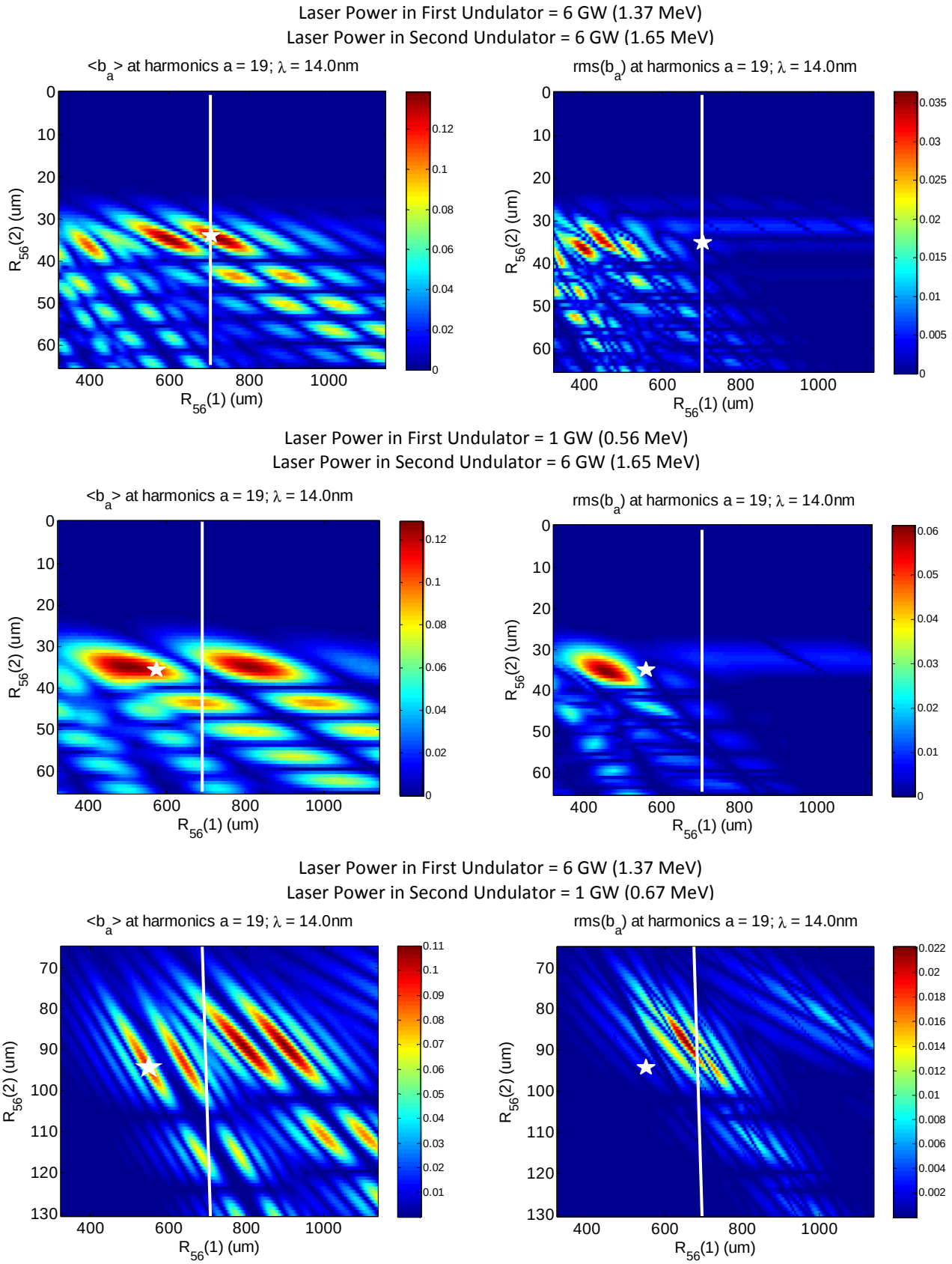

Figure 3: Average bunching factor and phase sensitivity of bunching factor for ranges of R_{56}s and for three different laser power combinations. Constants used include: a = 19, E_0 = 1.15 GeV, σ_E = 150 keV, λ = 270 nm. Working points plotted on following page (Fig. 4) are indicated by a star. The line represents the limit imposed by the vacuum chamber diameter.

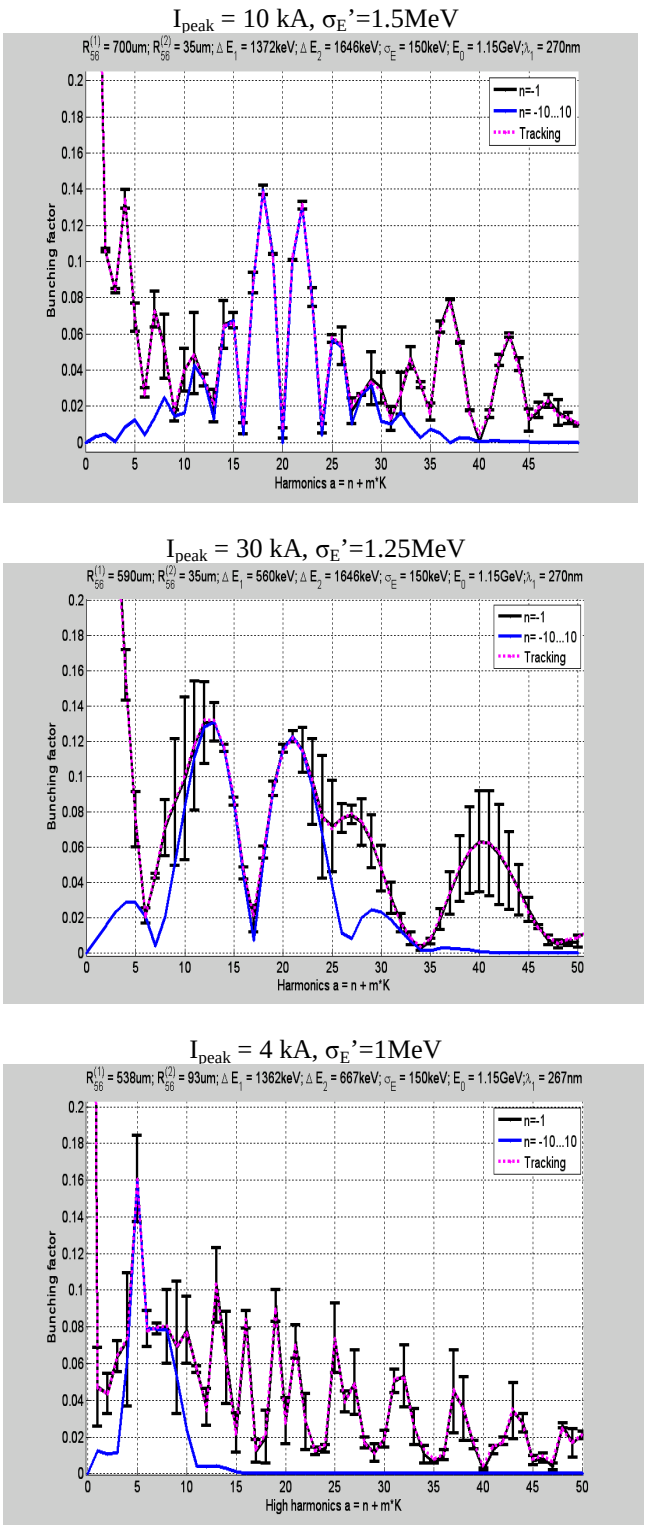

Figure 4: Bunching factor as a function of harmonic number for three different 14 nm ORS section EEHG – HGHG schemes indicated by stars on the plots from Fig. 3. The error-bars describe the rms sensitivity of each harmonic to changes in the relative arrival-times of the laser pulse and electron bunch. The peak current is written above each plot.

bunching and low phase sensitivity are desirable working points. The limit on the R_{56} of the first chicane imposed by the vacuum chamber diameter is indicated by a line and a selected operation point is indicated by a star. One can see that it is possible to find a operation point with small phase sensitivity, even in the vicinity of an island of large phase sensitivity. It is also apparent that slightly better operation points could be found for R_{56}s that exceed the limit imposed by the vacuum chamber. Given CSR and space charge effects, choosing operation points with low R_{56}s and low peak-currents is, nevertheless, prudent.

The bunching factor as a function of harmonic number for each of these operation points is plotted in Fig. 4 and the highest peak current for a microbunch is listed above the figure together with the rms energy spread after the EEHG process, which is given by,

$$\sigma_E' = \sigma_E \sqrt{1 + \frac{A_1^2}{2} + \frac{A_2^2}{2}}, \qquad (2)$$

where $A_1=\Delta E_1/\sigma_E$ and $A_2=\Delta E_2/\sigma_E$ [3].

Using the operation points indicated by stars in Fig. 3, the bunching factors predicted with the phase dependent bunching formula are plotted together with the phase independent n = -1 bunching factor prediction, Eq. 6 [1], and results from 1-D particle tracking. Excellent agreement is observed between the phase dependent bunching equation and the 1-D particle tracking results. The error-bars describe the rms sensitivity of each harmonic to variations in laser phase between the two undulators. This sensitivity, together with CSR sensitivity (peak current < 10kA) and energy spread (< $3\cdot10^{-3}$) are needed to determine an optimal working point.

From particle tracking, one can conclude that when the laser power is high (6 GW) in both undulator sections, as in the first case (top), one generates a large, 10kA peak current, large energy spread, and a large number of micro bunches per cycle of 270 nm. When the laser power in the first undulator section is low, as in the second case (middle), there are only a few microbunches per cycle of 270 nm and the 30 kA peak current of these microbunches is extremely high. When the laser power in the second undulator section is low, as in the third case (bottom), the 4 kA peak current is lower and there are more microbunches per cycle. This scheme possesses the longitudinal particle distribution which was plotted in Fig. 1 and it has a higher sensitivity to phase than the other two schemes, but it has the lowest peak current and energy spread.

While the top two working points would've been predicted by the n = -1 equation, the third and, due to the reasonable peak current and energy spread, perhaps the best working point would not have been apparent from the n = -1 equation and it would've been time consuming to find it through particle tracking alone. The main advantage of the phase dependent bunching formula, as it was used to make Fig.s 3 and 4, is that it predicts viable working points for low-R_{56} chicanes that would not

otherwise have been found. This is an important result for compact EEHG schemes.

Although only one harmonic number has been optimized here, a continuous and wide range of harmonics could be pursued with EEHG at FLASH. In contrast, the harmonics available for HHG at FLASH are constrained by the specific reflectivities of the XUV mirrors used to transport the beam. The disadvantage of EEHG compared to HHG comes in its sensitivity to electron bunch and chicane properties. These sensitivities will be explored in the following sections.

DIPOLE TOLERANCES

The transfer matrix elements R_{53} and R_{54} describe the longitudinal position of the electron as a function of its transverse offset or angle. Residual R_{53} and R_{54} after a chicane fold the transverse phase space into the longitudinal phase space, smearing out bunching in proportion to

$$\sigma_{z,y} = \sqrt{R_{53}^{\,2}\sigma_y^{\,2} + R_{54}^{\,2}\sigma_{y'}^{\,2}}\,, \qquad (3)$$

where and σ_y and $\sigma_{y'}$ are the rms widths of the position and angular spread of the electron beam and the β-function is constant. The R_{53}, R_{54} and smearing factor (Eq. 3) are plotted for each chicane (Fig. 5). One sees that for ideal magnet settings, the smearing factor should equal zero at the exit of each chicane. While a non-zero R_{53} or R_{54} is beneficial within the ORS chicanes, since it transversely smears out high peak currents which could give rise to instabilities, a non-zero R_{53} or R_{54} at the exit of the chicanes can have a detrimental effect on EEHG.

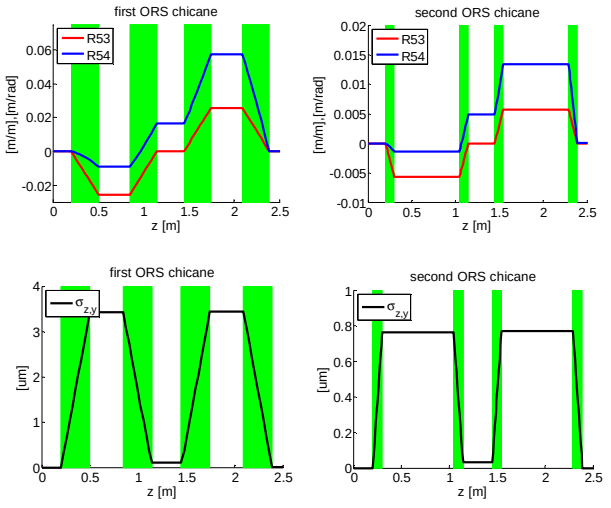

Figure 5: The R_{53} and R_{54} of the ORS chicanes (top) and the transverse smearing of longitudinal charge density spikes that they cause (bottom). Green bars represent magnet locations.

In order to develop a practical measure of the dipole tolerances, we must know R_{53} and R_{54} in terms of the dipole field errors. One starts by estimating that $R_{53} \approx$ the deflection angle of a dipole and $R_{54} \approx$ the transverse deviation from the straight ahead path. Then one can get,

$$R_{53} = \frac{2L_B}{\rho}\frac{\Delta B}{B}\,, \qquad (4)$$

where L_B is the [0.4 m, 0.1 m] magnet length, ρ is the [24.6 m, 13.1 m] bending radius, and ΔB is the rms error of the magnetic field in the bends [4].

$$R_{54} = \left(\rho\cdot\left(1-\cos\left(\frac{L_B}{\rho}\right)\right)+\frac{dL_B}{\rho}\right)\frac{\Delta B}{B}\,, \qquad (5)$$

where d is the [0.35 m, 0.75 m] distance between the first and second dipoles in the chicane and the approximation $\sin(\theta)\approx\theta$ has been used. For diagnostic purposes, it is interesting to note that these terms can be expressed in quantities which are easy to measure through beam-based dispersion measurement tools: $R_{53}=-R_{46}$ (or $\Delta z/\Delta y=\Delta y'/\Delta E$) and in the middle of the chicane $R_{54}=R_{36}$ (or $\Delta z/\Delta y'=\Delta y/\Delta E$).

One must now consider how the tolerance of magnet field errors is different in the first chicane compared to the second. One would expect that a non-zero R_{53} or R_{54} at the exit of the first chicane would only increase the effective slice energy spread of the microbunches, while at the exit of the second chicane, a non-zero R_{53} or R_{54} would cause the microbunches to tilt in the y-z plane.

A good way to estimate the magnet field tolerance for the first chicane is to derive an expression for the increase in the effective slice energy spread caused by a non-zero R_{53} or R_{54}. This is given by,

$$\sigma_{E(effective)}^{\,2} = \sigma_E^{\,2} + \Delta E^2 k^2 \sigma_{z,y}^{\,2}\,, \qquad (7)$$

where ΔE is the laser induced energy modulation, $k=2\pi/\lambda_r$, σ_E is the initial slice energy spread of the electron beam and $\sigma_{z,y}$ is the smearing factor from Eq. 3. One can then substitute $\sigma_{E(effective)}$ into the bunching equation (Eq. 1), in place of σ_E, and immediately see the dependence of the bunching factor on magnet field errors in the first chicane. The first chicane tolerance is very loose compared to that of the second chicane.

For the second chicane, a non-zero R_{53} or R_{54} at the chicane exit creates a y-z tilt of the microbunches, longitudinally smearing out the bunches. The effect of this smearing on the EEHG bunching factor can be written in terms of a microbunching suppression factor for a Gaussian bunch,

$$\frac{b_{noerror}}{b_{error}} = e^{\frac{1}{2}k^2\sigma_{z,y}^{\,2}}\,, \qquad (4)$$

where $k=2\pi/\lambda_r$ and $\sigma_{z,y}$ is the smearing factor from Eq. 3. A similar formula is given in [4] and it can be derived by substituting $z=R_{53}y+R_{54}y'$ into a 1-D formula for a longitudinally bunched distribution, $\ell(z)=1+\cos(kz)$, and then integrating over a Gaussian distribution.

One can specify $\sigma_{z,y}<\lambda_r/20$, a condition for which the microbunch is tilted by less than 5% of the radiated wavelength and for which the microbunching suppression factor is less than 1.025. For β=25 m, σ_y = 100 μm (rms) and $\sigma_{y'}$ = 5 μrad (rms), the magnet tolerance of the R_{53} term for generating λ_r = 14 nm with this condition would then be 0.02% for the second chicane, the tolerance for the R_{54} term would be 1%, and the net tolerance for the smearing factor Eq.3 would be 0.02%, dominated by the R_{53}. The magnet accuracy requirement is reduced when higher energy beams are used, since it scales with the geometric emittance and the 25 m β function used in the above calculation could be reduced to 5 m in order to relax the tolerances to 0.05%. Tuning the magnets with this accuracy will probably be the most challenging aspect of the EEHG experiment, due to the fact that the only applicable diagnostic of the quality of the microbunches is the seeded FEL signal itself.

There is a pair of quadrupole magnets on movers directly prior to the sFLASH undulator section and it is planned to use offsets of these magnets to provide a final correction to the R_{53} and R_{54}, such that even if the microbunches are slightly longitudinally tilted prior to the quadrupoles, they can be given a small correction directly prior to the undulator (Fig. 6). The magnets could function like a mini-dogleg. Ideally, the last ORS chicane would slightly undercompress the microbunches, and the mini-dogleg would provide the final compression.

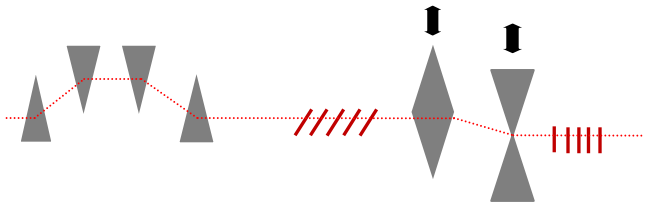

Figure 6: Small correction to longitudinal phase space given by tuning offset of quadrupoles prior to sFLASH undulator. Mini-dogleg can remove residual R_{53} and R_{54}.

This would be particularly good technique for combatting the detrimental effects of a high peak current. One such detrimental effect is CSR leakage, which acts like a nonlinearly z-dependent magnet field error. The big difference between the effect of a magnet field error and CSR is that the magnet field error acts uniformly over the entire bunch, while CSR acts non-linearly over the bunch. CSR will be discussed in the following section.

CSR EFFECTS

Coherent Synchrotron Radiation (CSR) could affect EEHG in three ways:

- the z-correlated energy spread itself
- projected emittance growth due to the CSR energy spread
- longitudinal smearing of fine structures through R_{53} and R_{54} leakage.

While all of these effects are cause for concern, the last is uniquely pertinent to EEHG and it could impact the bunch on both macro and microbunch length scales. There are codes like CSRTrack and ELEGANT which can calculate these effects, but because it is not clear if these codes are valid on the microbunch length scales which are critical for EEHG, an analytical treatment will first be pursued.

Steady-state calculations for 1-D CSR wakes are plotted below in Fig. 7. Fig. 7 (a.) is a wake for a macrobunch after the first chicane and Fig. 7 (b) is a wake for a microbunch in the last dipole. While the 1-D macrobunch wake is a somewhat realistic prediction and it tells us that 2.5 kA of peak current could be excessive for EEHG, the 1-D microbunch wake is a gross overestimate, due to the transverse smearing that occurs in proportion to R_{53} and R_{54} (Eq. 3, Fig. 5) and due to the fact that the high peak current is not produced until the very last few millimeters of the dipole.

(a.) CSR wake from 1-D macro-bunch in first chicane

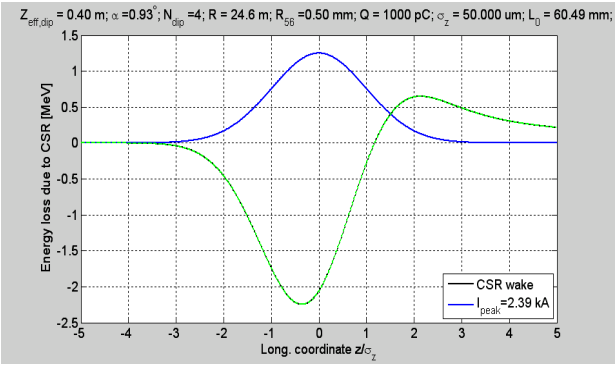

(b.) CSR wake from 1-D micro-bunch in last dipole

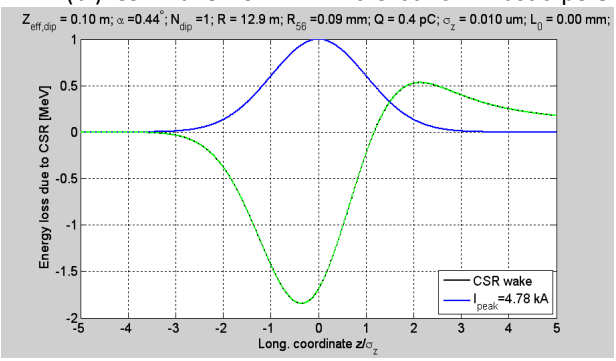

Figure 7: CSR wake from the first chicane on the macro-bunch (a.). CSR wake from the last dipole of the second chicane on a 1-D micro-bunch (b.). Key parameters: dipole length, bending angle, number of dipoles, bending radius, dispersion, charge, bunch length, and overtaking length are listed above each plot.

It has been verified that high peak currents only occur in the first chicane in regions with significant transverse smearing. The danger for micro-bunch CSR arises at the exit of the second chicane, where the smearing goes to zero and the peak current reaches its highest value. That is why it would be wise to slightly undercompress the microbunches in the last chicane and produce the last fraction of compression in the mini-dogleg arrangement depicted in Fig. 6.

For the macro-bunch, the CSR induced deviations in the energies or transverse positions of longitudinal slices can reduce the length of the portion of the electron bunch which will have the energy and energy chirp which is suitable for seeding. While one expects an energy chirp due to the compression process, the energy chirp produced through CSR is non-linear and only linearly chirped portions of the bunch are usable for seeding.

Comparisons of the 19th harmonic ORS-EEHG CSR wakes and chicanes with 20th harmonic FLASH II CSR wakes and chicanes show many similarities. For practical purposes, the chicanes and wakes are identical. In 3-D CSRtrack simulations for FLASH II EEHG [7], CSR in the first chicane was shown to reduce the bunching factor at the 20th harmonic by about half for a 1.5 kA beam. The reduction was even greater for a 2.5 kA beam. In ORS-EEHG, the same behavior should be expected, but the authors believe that the reduction in the bunching factor observed in the FLASH II simulations was caused not by variations in the energy of various beam slices as was postulated in [7], but by R_{53} and R_{54} leakage which caused the microbunches to be slightly undercompressed. The authors believe that given different magnet settings, this effect could be completely suppressed for at least a portion of the bunch. Magnet settings which fully suppress the CSR leakage for a portion of the bunch would add a negligible amount of energy dependent position jitter.

Given the complex and sensitive dependence of the bunching factor on dipole settings and CSR, a systematic tuning procedure must be developed. It is anticipated that this will be the most challenging aspect of the experiment.

ISR EFFECTS

For large enough chicane bending angles and beam energies, Incoherent Synchrotron Radiation (ISR) could increase the slice energy spread of the beam in the first chicane. The energy spread generated by ISR after passing a dipole is given by [14],

$$\Delta\sigma_E = 6.4[keV] \cdot \sqrt{\frac{L[m]}{R[m]^3}} E[GeV]^{7/2}$$

Where R is the bending radius, L is the dipole length, and E is the beam energy. In our case, the ISR energy spread is about a keV and is insignificant compared to the energy modulation from the laser.

RADIATOR TOLERANCES

The sFLASH undulator section consists of 4 variable gap undulators with a total of 300 periods. The limitation on the undulator gap, as imposed by the vacuum chamber height requires that the seeded wavelengths must be shorter than 17 nm for any EEHG scheme to work at 1 GeV (Fig. 8).

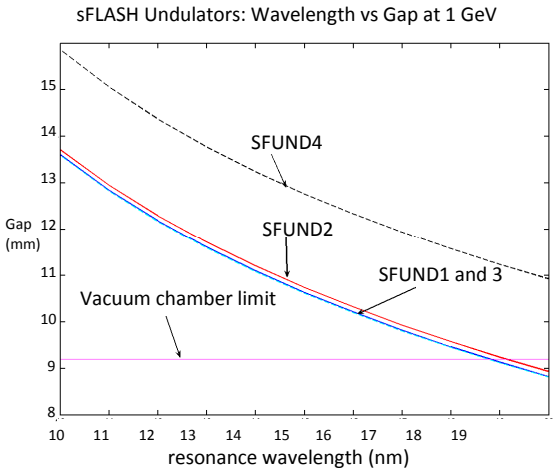

Figure 8: The wavelength vs. gap at 1GeV for the four sFLASH undulators. The undulators cannot be closed beyond the vacuum chamber limit. This plot was provided by H. Delsim-Hashimi (DESY)

Thus, the scheme to produce 14 nm in the sFLASH undulators will not require an overly small undulator gap.

The bunching factors and energy spreads generated with the 1-D EEHG tracking code were used as input parameters for the FEL code GENESIS [15]. The goal was to simulate the radiation which might be produced in the sFLASH undulators for different energy spreads, bunching factors and peak currents. The beam parameters used in the simulation were uniform along the entire bunch. The emittance was 1.5 mm·mrad, the β function was 6 meters in x and 7 meters in y, α was equal to zero, and the beam energy and undulator parameter were tuned so that 14 nm radiation would be produced.

The radiation and bunching produced in the first 3 sFLASH undulator sections was simulated for an electron beam with a peak current of 2.5 kA and a range of energy spreads and bunching factors. These results are plotted in Fig. 9, predicting that the planned operation point with a 1 MeV energy spread will reach saturation within the four undulator sections. If the peak current is 1.5 kA instead of 2.5 kA, the peak power achieved after 3 undulator sections with a bunching factor of 0.1 and an energy spread of 1 MeV is 1 GW instead of 3.5 GW. Improved performance for beams with a high initial bunching factor could be achieved through adjustment of the phases of the undulators, but this was not done in the simulations shown in Fig. 9.

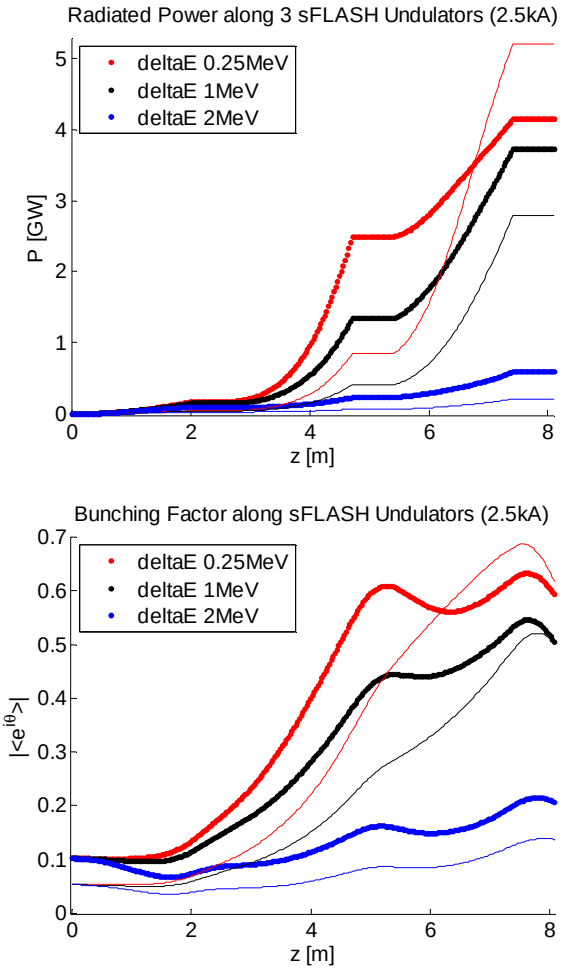

Figure 9: Power and bunching levels in the first three sFLASH undulators for ORS-EEHG seed with a peak current of 2.5 kA and different initial energy spreads and bunching factors. The thick lines are for an 0.1 initial bunching factor and the thin lines are for an 0.05 initial bunching factor.

It should be noted that the accuracy of GENESIS for EEHG bunched beams has not been benchmarked. It is, however, known that it is more accurate to enter the bunching factor as a constant in the input file for a flat current distribution than to directly import a bunched current distribution. Importing a bunched particle file leads to gross overestimates of the radiated power for a given bunching factor [16].

These simulated beams consisted of unrealistic, perfectly linear, flat bunches where every portion of the bunch lased with an equal amount of power. Realistic, curved, chirped electron bunches would be seeded with a distorted, chirped laser which would only overlap with a fraction of the bunch. These effects were not simulated with GENESIS and will be described in the following section.

REALISTIC ELECTRON BEAM

The electron beam at FLASH is typically produced with either roll-over compression or linearized compression. While roll-over compression produces a very sharp peak of high charge density followed by a long trailing tail, linearized compression should, in principle, produce a beam which is uniform in charge density and other properties. The reality is that while linearized compression is about 4 times better than the roll-over compression in terms of bunch uniformity, the electron bunch in linearized compression still typically has a peak of current, followed by a region over which the current decreases to half of the peak value. This is generally true for standard operation and peak currents in the range from 1 to 2.5 kA, but it should be noted that a wide range of bunch shapes are possible for different operation configurations and low bunch charges.

The slice energy spread along the bunch is also not uniform. It peaks at the head of the bunch and falls off to a low of 250 keV located in the middle of the bunch. The peak slice energy spread depends on the peak current and can range from 0.75 MeV for a 1 kA peak current to 4 MeV for a 1.5 kA peak current and so on upwards. This has been studied by C. Behrens (Fig. 10) [17].

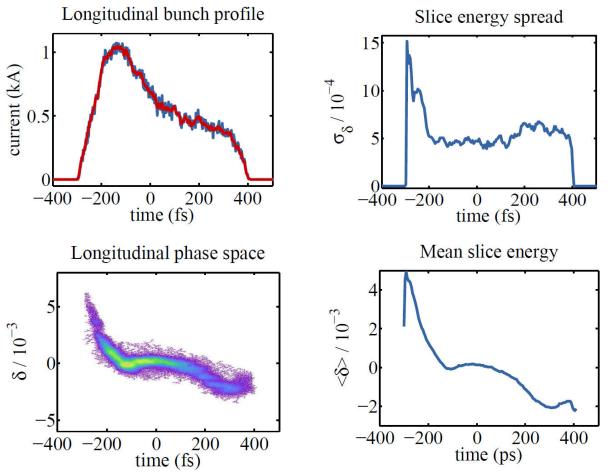

Figure 10: Measured slice energy spread (left), and deviation of the slice energy from the nominal (right). From C. Behrens [17].

For the charge distribution shown in Fig 10, a reasonable portion of the bunch to seed might be a 50 fs long region near the head of the bunch with the lowest energy spread and a high enough peak current. In comparison, for the charge distribution shown in Fig. 11, taken from an HHG experiment run [18], a reasonable portion of the bunch to seed would be a 100 fs long region in the center of the bunch. The bunch distribution shown in Fig. 10 would probably be preferable in situations where the SASE background overwhelms the emerging seed radiation signal.

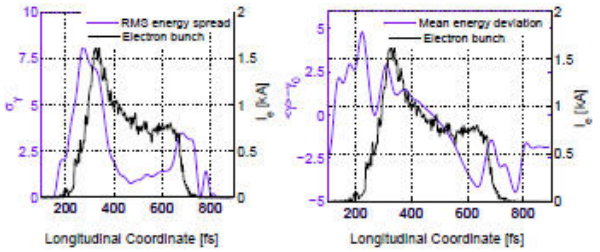

Figure 11: Longitudinal charge distribution of electron bunch plotted together with measured slice energy spread (left), and deviation of the slice energy from the nominal (right). From R. Tarkeshian et al., Proc. of PAC'11 (New York) [18].

The transverse beam size also has an impact on the performance of the EEHG experiment. In Fig. 12, the β-function for a typical HHG run was plotted by V. Milchev.

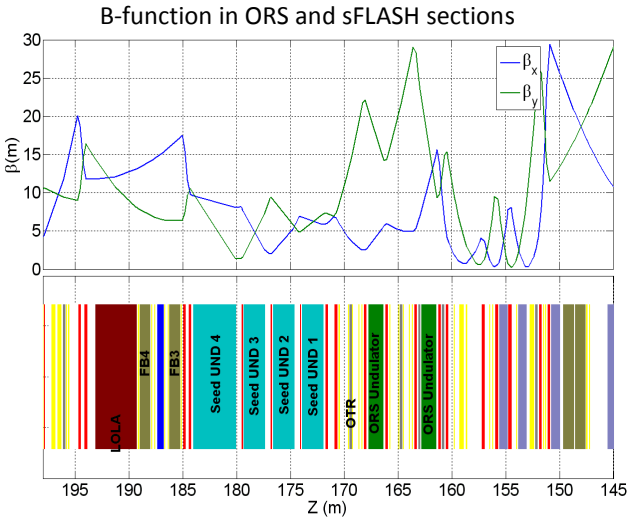

Figure 12: Beta function in ORS and sFLASH section plotted for HHG run by V. Milchev (DESY). The beam direction is from right to left.

Since the EEHG experiment will attempt to run parasitically there will not be much opportunity to completely change the optics. For the HHG experiment, the β_y-function is relatively large in the ORS section, and in order to combat R_{53} and R_{54} leakage and the effects of transverse laser distortions it would be wise to reduce the β-function in that region. Nevertheless, the current β-function of ~25 m would make a <100 μm (rms) electron beam radius and this would be ~3 times smaller than the expected laser spot size, and this is small enough to avoid large scale laser distortions.

INCOMING SLICE ENERGY SPREAD

For some EEHG schemes, the sensitivity to slice energy spread is large, for others it is not. The incoming slice energy spread dependence of a scheme to generate the 19th harmonic of 270 nm is plotted below in Fig. 12. This scheme uses 6 GW of laser power in the first undulator and 1 GW in the second. As the incoming slice energy spread is increased from 150 keV to 550 keV, the peak current of the individual microbunches is reduced. The bunching factor and the sensitivity to changes in the phase of the laser is also reduced.

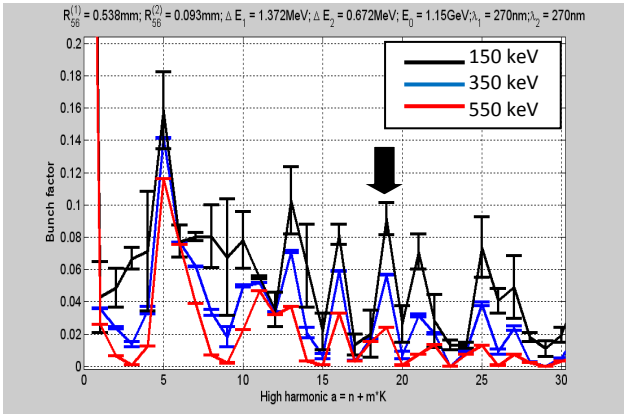

Figure 12: The bunching factor as a function of harmonic number for three different incoming slice energy spreads: 150 keV, 350 keV, and 550 keV; K=1.

For a different scheme to generate the 19th harmonic of 270 nm in which 6 GW of laser power was used in both undulators, the reduction in the bunching factor resulting from increases in the incoming slice energy spread is significantly smaller (Fig. 13). But this comes at the cost of creating a much larger slice energy spread and peak current going into the radiator undulators. In this figure, it is easier to see how the increase of the slice energy spread affects the higher harmonics before it affect the lower harmonics.

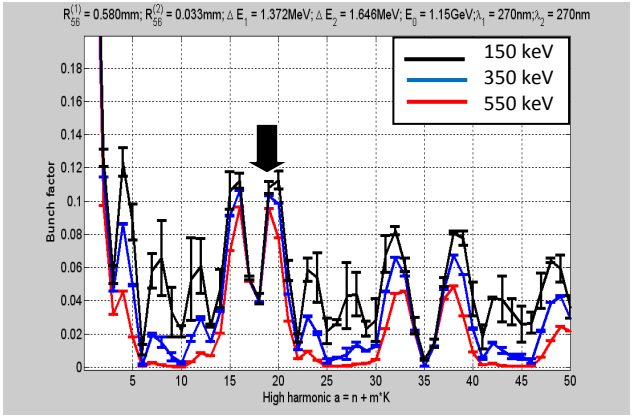

Figure 13: The bunching factor as a function of harmonic number for three different incoming slice energy spreads: 150 keV, 350 keV, and 550 keV; K=1. More laser power was used in the second undulator in this scheme.

CHIRPED LASER BEAMS

For a given operation point, a small change of the seed wavelength produces a small change in the output bunching period, but the bunching factor does not change appreciably. Consequently, chirped seed laser pulses result in chirped bunching distributions.

If the bunching bandwidth is larger than the bandwidth of the sFLASH undulators and if the bunching has a substantial frequency chirp, only a slice of the bunch will lase. If we can control this chirp, it would provide a mechanism for tuning the length of the seeded FEL pulse. The FEL bandwidth is ~0.5% and the maximum EEHG bandwidth is 5%. If the EEHG pulses were maximally chirped with a maximum bandwidth and a length of 300 fs (FWHM), then 30 fs of that pulse would be usable for seeding in a given operation setup. The present EEHG seed generation scheme will produce 100 fs (FWHM) pulses with an expected bandwidth of 0.6% [12] and cannot be used to test the chirp-slicing concept. Due to the shortness of the pulses, however, one would only expect the central 50 fs of the pulse to have an intensity appropriate for seeding. The main advantage of having a longer, chirped laser pulse is not in the length of the pulses which can be produced, but in the reduced sensitivity to changes in the energy of the electron bunch. Compared to a non-chirped laser pulse, a chirped pulse simply has a wider range of *correct* seed wavelengths for a range of electron beam energies.

CHIRPED ELECTRON BUNCHES

A chirped electron bunch has a different effect on the EEHG process. If an electron bunch with an energy chirp is given an energy modulation and it is then compressed in a chicane, it will develop a different bunching period than that which would be generated with an unchirped electron beam. As long as the radiator undulator is tuned to radiate at this particular bunching period, the electron bunch chirp should pose no problem. With a non-linear chirp, which, due to collective effects or imperfect RF settings, is frequently the case at FLASH, despite the operation of the 3rd harmonic module, one would expect that the portion of the bunch which would be usable for EEHG would be reduced as described in the previous section.

The easiest way to check the magnitude of this chirp effect is to change the electron beam energy by small amounts in the simulation and see how the bunching factor is affected. A scan of the beam energy over a 10% range in Fig. 14 shows a low sensitivity to beam energy changes. It shows disagreement between the 1-D tracking and the n=-1 analytic bunching formula probably due to inaccuracies in the low-R_{56} regime. Trusting that the particle tracking result is more accurate, one can conclude that ~1% energy changes from the goal energy can be tolerated without affecting the bunching factor at all and 5% changes can be tolerated with only a mild effect on the bunching factor. Even if we tune the radiator undulators to an energy which is 5% away from ideal, the EEHG process should still be effective. The 1%, energy chirp limit imposed by the collimator is, however, more severe.

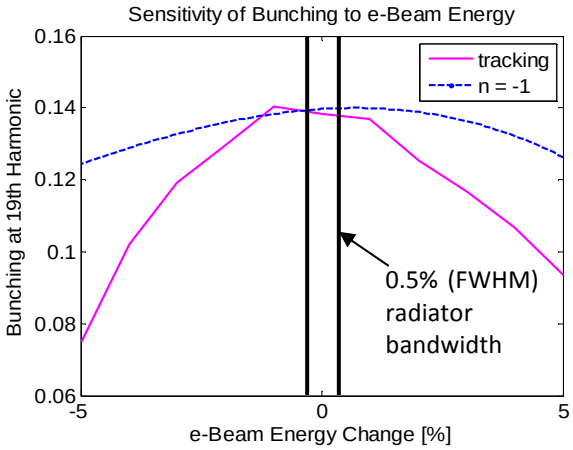

Figure 14: The bunching factor as a function of e-beam energy for the 19th harmonic of 270 nm. The sensitivity of a range of EEHG operation points to changes in beam energy is largely uniform and weak. The bandwidth of the sFLASH radiator undulator will determine the sensitivity of EEHG to beam energy changes and not the EEHG process itself.

LASER PHASE NOISE

We have shown the sensitivity of this EEHG scheme to changes in the phase of a perfect laser pulse relative to the electron beam (Eq. 1), but we have not shown the impact from changes of the phase of the laser pulse within the pulse itself. There may be a hard-limit on the harmonics that can be achieved, as determined by the phase noise within a laser pulse. This sort of phase noise is impossible to measure with known methods and its impact on HGHG was postulated in [19] with an argument which is simplified as follows:

- bunching ~ $e^{in\omega t}$
- add phase noise ~ $e^{in(\omega t+\varphi)}$
- emitted power ~ $(e^{in(\omega t+\varphi)})^2$

Therefore, there is an amplification of the noise in proportion to the harmonic number squared. In terms of the signal-to-noise ratio, this looks like,

$$\left(\frac{P_s}{P_n}\right)_{out} = \frac{1}{n^2}\left(\frac{P_s}{P_n}\right)_{in}.$$

While there are two harmonic numbers in EEHG (n and m), it seems logical that a similar line of argumentation might be taken to anticipate the phase noise impact on EEHG. According to this hypothesis, if there is a phase noise of φ within the 800 nm laser pulse, then the frequency tripled pulse would have a phase noise of φ*9 and the 20th harmonic of this pulse would then have a phase noise of φ*180.

This hypothesis is borne out by particle tracking simulations in which phase noise was added to the energy modulation. In Fig. 15, the bunching factor for a range of seed laser phase noises is plotted.

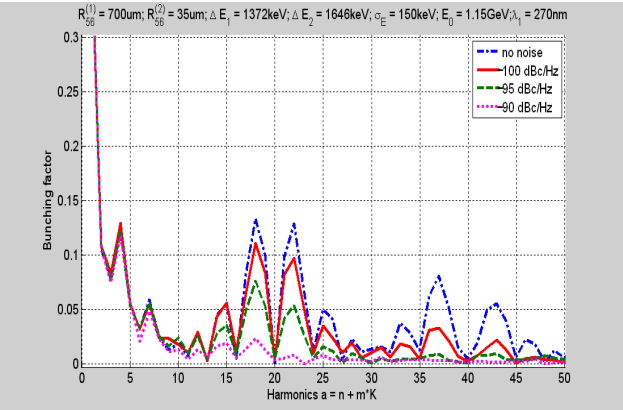

Figure 15: The bunching factor for several different amounts of laser phase noise. The high harmonics are affected by the phase noise first. The phase noise threshold is sharp and not gradual.

A simple VCO phase noise model was used with a bandwidth of a few GHz, in which the phase noise is mixed with the carrier to produce sidebands around the carrier. It is not clear if this is an accurate representation of the phase noise of the laser, since it can't be measured. Despite this, it is clear that this phase noise will impact the higher harmonics earlier than it does the lower harmonics. The impact of phase noise on the bunching factor manifests as a sudden drop off at a certain noise threshold. The effect might be reduced by slippage of the seed pulse through the bunch, but this isn't entirely clear.

LASER AMPLITUDE NOISE

As long as the seed laser power is optimized for a given operation point, the laser amplitude noise will not have a strong effect on the EEHG bunching factor, as shown below in Fig. 16. Changes of the laser power by as much as 20% change the bunching from 0.14 to 0.08. A FWHM laser amplitude stability of 5% should be expected, producing practically no jitter in the bunching factor when the laser power is optimized for a given harmonic. If the laser power is not optimized, then the sensitivity to laser amplitude would grow in proportion to the deviation from the optimum.

One can also use this result to calculate the longitudinal portion of the seed laser pulse which would be usable for seeding. The length of the laser pulse for which the amplitude does not vary by more than 20% from the peak value is about 50 fs for a 100 fs (FWHM) seed pulse. This means that about 50 fs of the seed pulse would have a power level sufficient for seeding.

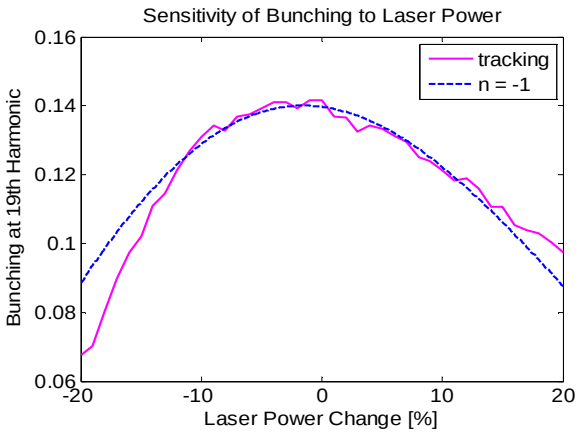

Figure 16: The bunching factor as a function of laser power for the 19th harmonic of 270 nm. The parameters from the first scheme from Fig. 3 were used, but the sensitivities of the other schemes were similar.

LASER WAVEFRONT DISTORTION

The quality of the 270 nm seed wavefronts will directly affect the quality of the echo-seeding microbunches. While small tilts of the microbunch which result from tilts of the wavefront can be compensated with adjustments of the chicane dispersion, more complicated distortions like those shown below in Fig. 17 will directly degrade the bunching factor of the goal harmonic, effectively smearing out the peaks of high peak-current. An easy estimate for the tolerance is ~10% of the radiated wavelength. For the 20th harmonic of 270 nm, the tolerance would be ~1 nm.

To simulate the problem, one can directly model the fields of a 3-D laser beam with multiple transverse higher order modes, or one can do a much easier 1-D approximation in which several runs of 1-D particle tracking through the ORS section are conducted, each time changing the initial phase of the laser by a slight amount, and each time saving the final particle distribution as a function of that phase. If one chooses a selection of initial phases which represent the geometry of a likely wavefront distortion (Fig. 17), one can then concatenate those particle distributions together in order to calculate the bunching factor for a distorted wavefront.

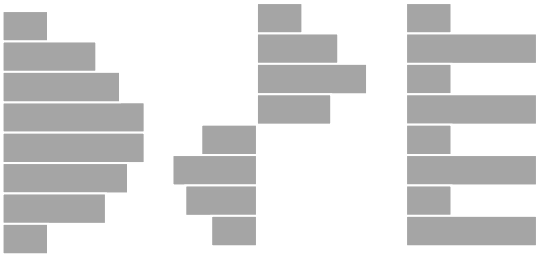

Figure 17: Possible wavefront distortions.

But then it becomes clear that the shape of the distortion is irrelevant and the magnitude is what is important. We can define the magnitude as the rms deviation from a flat

wavefront and perform the calculation with a random assortment of phases with a given rms deviation from zero.

This process of averaging over various phases sounds very similar to what was done for Fig. 4, in which the sensitivity of EEHG to a laser phase which is not the same in both undulators was calculated, but it is not. For Fig. 4, the bunching factor was calculated as a function of phase and then averaged, whereas for Fig. 18 (below), the distribution is calculated as a function of phase and then averaged before calculating the bunching factor.

In Fig. 18, the bunching factor for a range of wavefront distortions was calculated for two different operation points and similar sensitivity to wavefront distortions was observed. The wavefront distortion was only added to the laser in the second undulator.

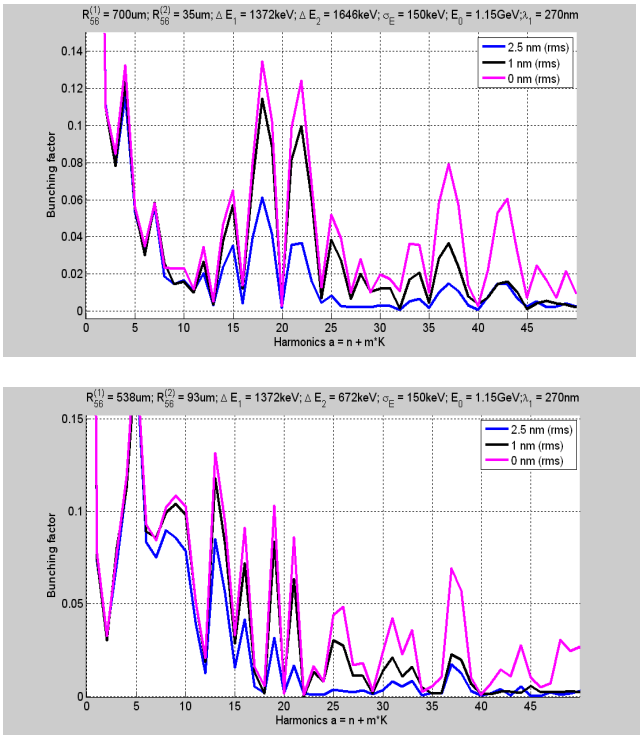

Figure 18: The bunching factor for 0, 1 and 2.5 nm (rms) wavefront distortions calculated with particle tracking approximation. The distortion was only added to the laser in the second undulator.

Wavefront distortions have a much stronger effect if they occur in the second undulator than if they occur in the first undulator. The impact in the first undulator is not, however, negligible, for some operation points. The operation point shown on the top in Fig. 18 is relatively insensitive to wavefront distortions in the first undulator, but the operation point on the bottom shows some slight sensitivity: the 2.5 nm (rms) wavefront distortion reduced the bunching factor by ~10%, a small amount compared to the reduction produced by the wavefront distortion in the second undulator.

To analytically describe the influence of a distorted 270 nm laser wavefront in the second undulator on the EEHG bunching factor, one can use the theory developed for describing the influence of magnetic chicane errors on EEHG (Eq. 4) to get the bunching factor suppression as a function of distortions of the 270 nm seed (λ_s),

$$\frac{b_{error}}{b_{noerror}} = e^{-2\pi^2 a^2 \left(\frac{\Delta\lambda_s}{\lambda_s}\right)^2} \qquad (2)$$

Where a is the harmonic number The suppression factor for a range of harmonics and wavefront distortions is plotted in Fig. 19.

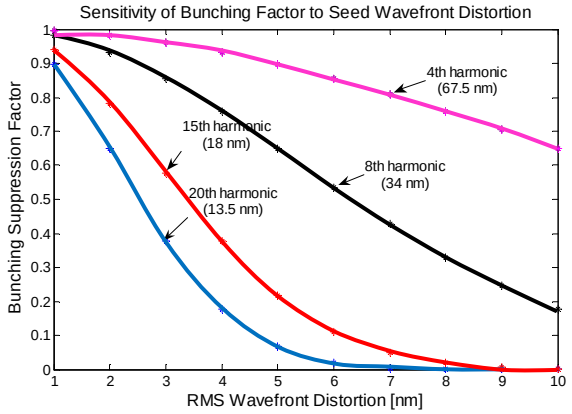

Figure 19: The bunching suppression factor for a range of harmonics and wavefront distortions.

From Fig. 19, one sees that the wavefront quality requirement increases dramatically as one attempts to reach higher harmonics. Wavefront control and spatial filtering techniques for addressing these very difficult tolerances are described in [12], but it was noted that even if a wavefront sensor could get <2 nm wavefront resolution, it would need to installed after a mirror and a window. As a result, the sensor ends up measuring the flatness of the window. If one can tune directly on the FEL beam itself, however, then one has the most sensitive measurement available. If one tried to tune the wavefront for the 19th harmonic on the FEL beam signal, one might never find the signal at all, but if one started with HGHG at the 7th harmonic (Fig. 20), there would be a very good chance to use the signal to optimize the wavefront.

Besides being a useful wavefront tuning technique, HGHG at the 7th harmonic (38.5 nm) is the same wavelength pursued by the HHG experiment, enabling ease of switching between the two experiments. Compared to EEHG, HGHG is also considerably easier in terms of synchronization and chicane tolerances. Based on the sensitivity of HGHG to the slice energy spread, it appears that HGHG will have a high chance of success with the ORS section (Fig 20). The likely 250 keV energy spread will not be too large for a significant bunching factor at 38.5 nm to arise.

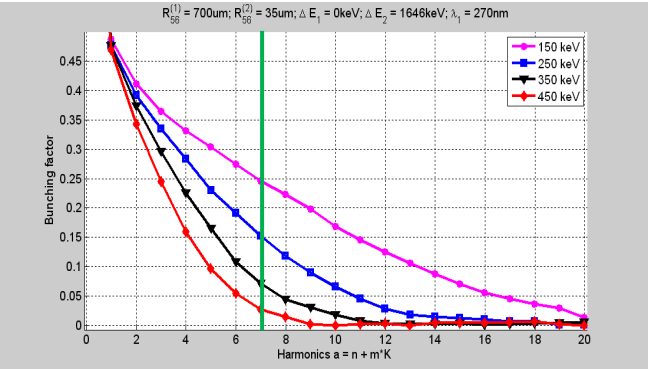

Figure 20: The rms slice energy spread sensitivity of HGHG in the ORS section at the 7th harmonic of 270 nm.

INCOMING MICROBUNCHES

The microbunching which develops prior to the ORS section could also have an impact on the echo-seeding experiment. The incoming microbunching has a broadband character ranging from <300 nm up to 20 μm in a continuous arc, peaking with a form factor (~bunching factor) of 0.005 at a wavelength of 10 μm [20,21]. These structures are present regardless of whether or not the bunch is off-crest and they increase for smaller emittances and larger peak currents. In the THz range, the microbunching increases with larger R_{56}s [20]. In the visible range, an opposite behavior is observed: the microbunching decreases with larger R_{56}s [21]. This is possibly due to the fact that, in the visible wavelength range, the non-zero R_{51}s and R_{52}s of the chicanes will cause microstructures to be smeared out in proportion to the R_{56}, leading to an increase in microbunching in the visible as the R_{56} is decreased.

What this means for EEHG is that the weaker bunch compressor settings which have been used for linear compression with the 3rd harmonic module could exacerbate any problems posed by microbunching. Compared to roll-over compression in which any substructures would be smeared out due to the energy spread, in linearized compression, the beam is under compressed, potentially amplifying substructures instead of smearing them [23]. For linear compression, one should expect a microbunching gain in the range of a few hundred, amplifying the 10^{-4} shot-noise throughout the visible part of the spectrum [24].

The problem that incoming microbunches pose for EEHG is that the incoming bunching may be stronger than the bunching induced by the seed laser and depending on the phase of the incoming bunching relative to the seeded bunching, a dramatically different laser power would be required to correctly fold and bunch the affected portion of the beam. The length of the affected portion of the beam is determined by the coherence length of the incoming microbunching. Based on measurements of the number of modes present for a given microbunching wavelength, it was determined that for 550 nm, 70-80 modes are present in a given bunch and for 1350 nm, there are only ~15 [25]. This means that for any given wavelength, there are many different regions radiating coherently and independently at any given time, and if one assumes a 50 μm long bunch with 100 modes at a wavelength of 500 nm, the maximum length of any coherently radiating segment would be equal to the length of a single 500 nm wavelength. This means that for EEHG, the incoming microbunches would interfere constructively or destructively with the seed laser modulation, varying from cycle-to-cycle. It is unknown whether this cycle-to-cycle variation is purely random or if it varies continuously throughout the bunch.

Such random variation occurring at 270 nm would be disastrous for EEHG, were it not for the fact that microstructures below 600 nm can be completely smeared out in the dogleg under typical optics configurations [26]. It is still possible that the 3rd harmonic of an 800 nm microbunched structure could radiate in the ORS undulators, disrupting the EEHG modulation, but odd harmonics radiate on axis with a power which is much weaker than the fundamental [27], so we do not expect a significant impact from this.

One could search for substructures using the "trickle-heating" effect [28] where for lower laser power levels, the laser beam drives an existing collective instability and achieves a modulation which is much higher than that which one would expect from the laser alone. For example, at LCLS, the expected energy modulation for a given laser energy is 7.5 keV but the effective modulation is 28 keV. EEHG will be operating in the 1 MeV energy modulation range, so this sort of effect is not expected for typical operation.

COMPARISON WITH FLASH II EEHG

While the <0.7 mm ORS R_{56} is small, it is not very different from the 1 mm R_{56} chosen for 0.7 GeV FLASH II EEHG scheme to reach the 20th harmonic of 260 nm. One only needs a several millimeter R_{56} in the first chicane if one is trying to generate higher harmonics with a modest amount of laser power and with a minimum of phase sensitivity. Table 1 lists the basic parameters of some planned EEHG experiments, along-side potential 2012 ORS EEHG parameters.

facility	E_0 *(GeV)*	$R_{56}^{(1)}$ *(mm)*	$R_{56}^{(2)}$ *(mm)*	λ *(nm)*
FERMI FEL2	1.2	8.2	0.35	4
FERMI FEL2	1.2	2.5	0.12	10
FLASH II	1.2	5.2	0.09	4.37
FLASH II	0.7	1.1	0.06	13.1
FLASH I ORS	1.15	<0.7	<0.1	10-40
FLASH I ORS	0.7	<0.7	<0.1	10-40

Table 1: Parameters of some planned EEHG experiments, along-side some potential 2012 ORS EEHG parameters. The seed wavelength for all of the experiments is ~250 nm.

While the R_{56}s in the table vary significantly, the difference in the laser powers required by each of the schemes from Table 1 is more striking:

- -FERMI FEL2 [250 MW]
- -FLASH II [1.5 GW]
- -FLASH I ORS [6 GW]

The ORS section is unique in that a laser capable of delivering high power levels on a single-bunch basis is already operational and injectable. This laser is described in the context of the seed properties in [12].

CASCADED HGHG

An FEL using High Gain Harmonic Generation (HGHG) is composed of at least two undulators separated by a chicane and it has been proposed to utilize the HHG seed in the sFLASH undulators to seed radiation in the FLASH SASE undulators using a fresh-bunch cascade technique [29,30]. This same concept could also be applied to echo-seeding with the sFLASH undulators. The idea behind the fresh-bunch technique is that the seeded portion of the bunch is too heated to be used to radiate in a second undulator stage, so the radiation from the first stage must be positioned over a fresh, un-modulated portion of the bunch [31]. The challenge of the technique is to overlap the radiation from the head of the bunch with an appropriate portion of the tail of the bunch; as a result, the technique often requires long, high-charge bunches or very short seed pulses.

Since the echo-seeding experiment being prepared for 2012 would heat a 100 fs long portion of the electron bunch, the chicane after the sFLASH section would have to delay the electron bunch relative to the FEL radiation by ~100 fs, requiring an R_{56} of ~60 μm, a value which is achievable with the existing chicane. If one wishes to forgo the use of this chicane over concerns about microbunching instabilities, one can attempt the super-radiant cascade technique [32,33]. In this technique, the modulation, debunching, and bunching all happen simultaneously at different locations within the bunch and the result is an extremely short pulse of radiation with degraded spectral quality.

For any HGHG scheme to work, the radiation intensity from the sFLASH undulators must be sufficient to seed in the SASE undulators. Based on the GENESIS simulations presented in a previous section and on the equation for the opening angle of undulator radiation for harmonics *m*,

$$\sigma_{\theta,m} = \frac{1}{\gamma}\cdot\sqrt{\frac{1+K^2/2}{2mN_u}}, \qquad (5)$$

[34], the radiated 14 nm beam size at the exit of the sFLASH undulators would be ~100 μm (rms) and the divergence would be ~40 μrad (rms). The 3rd harmonic of 14 nm would have a smaller beam size, divergence and power. One can derive an expression for a harmonic's power from the spectral density per electron of the radiation emitted in the forward direction for the m^{th} harmonic [27],

$$\frac{d^2U_m}{d\Omega d\omega} = \frac{e^2\gamma^2m^2K^2}{4\pi}\cdot\frac{\sin^2\left(\pi N_u(\omega-\omega_m)/\omega_1\right)}{\sin^2\left(\pi(\omega-\omega_m)/\omega_1\right)}\cdot|JJ|^2$$

where

$$JJ = J_n\left(\frac{mK^2}{4+2K^2}\right) - J_{n+1}\left(\frac{mK^2}{4+2K^2}\right),\ m=2n+1.$$

The radiated power for a given harmonic is proportional to the spectral energy [27],

$$U_m(\omega) = \frac{d^2U_m}{d\Omega d\omega}\Delta\Omega_m \qquad (6)$$

contained in the solid angle $\Delta\Omega_m=2\pi\sigma_{\theta,m}$. Within this solid angle, the ω dependent frequency shift is less than the bandwidth of the radiation. Upon closer inspection, one can see that the ratio of the power radiated at the m^{th} harmonic compared to the power radiated at the fundamental is dependent only on *K* and *m*, and not on γ or λ_u. If one plots U_m as a function of radiated wavelength for the sFLASH undulators with *K*=2.66, as was used in the 14 nm EEHG scheme, one sees that the 3rd harmonic has about half of the spectral energy of the fundamental radiation within the solid angle defined by Eq. 5 (Fig. 21).

Due to the possibility of residual bunching from the EEHG process, it should be considered that Eq. 6, the energy per unit bandwidth, from an incoherent beam, could be an underestimation of the available HGHG seed power [35]. One could use the residual bunching factor at the (3·19=) 57th harmonic of 270 nm in order to estimate the enhancement at the 3rd harmonic of 14 nm which could be achieved compared to an incoherent beam. This bunching factor could fall anywhere between 0 and 0.05, depending on the operation point.

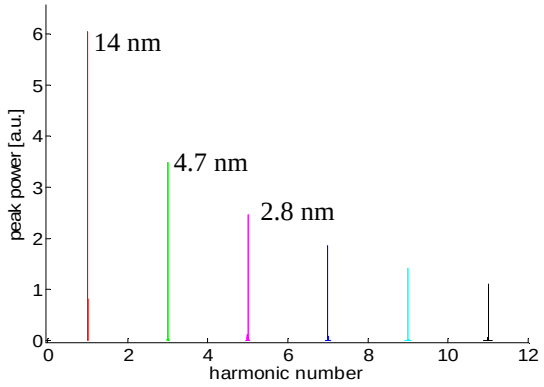

Figure 21: The spectral energy of the m^{th} harmonic emitted into the solid angle $\Delta\Omega_m$. The Lorentz factor is γ = 2250, the undulator period is λ_u = 3.14 cm, and the *K* parameter is 2.66.

Based on Eq. 5, at the beginning of the SASE undulators, 20 meters after the sFLASH undulators, a reasonable approximation for the 3rd harmonic beam size would be 200 μm (rms). Based on Eq. 6, one would expect the 3rd harmonic to have half of the 1 GW fundamental peak power for a 1.5 kA electron beam. If the intensity coming directly out of the sFLASH undulators is $500MW/(pi*100^2\mu m^2) = 6\ GW/cm^2$, by the time it reaches the SASE undulators, it would be a $500MW/(pi*200^2\mu m^2) = 1.5\ GW/cm^2$ with a peak power of 120 MW.

For a frame of reference, 100 kW is the peak power required to see a factor of 10 difference between the SASE background and HHG seeded radiation in the sFLASH experiment, while 1 kW is insufficient power to generate a seeded beam which has more pulse energy than the SASE background [18]. More specific criteria for seed power are given in [36], requiring 1 MW ($8\cdot10^8\ W/cm^2$) for seeding at ~5 nm. This is the seed intensity required to suppress fluctuations of the higher harmonics and it is several orders of magnitude higher than the intensity required to merely establish temporal coherence [36].

From these criteria, one could conclude that if echo-seeding at 14 nm with the ORS-section is successful, HGHG with the SASE undulators has a high likelihood of success for the 3rd harmonic; the predicted harmonic intensities are several orders of magnitude larger than required for successful seeding. Unfortunately, even though there could potentially be enough sFLASH radiation to use HGHG to seed up to the 9th harmonic of 14 nm, the FLASH SASE undulators have a fixed gap and cannot be opened more in order to accommodate harmonics higher than the 3rd.

The SASE undulators can also not be moved out of the beam path, so the SASE background would be a problem for HGHG schemes with higher peak currents. If the peak current used for EEHG is reduced to ~1kA a better signal to noise ratio could be achieved, due to the fact that the SASE would not reach saturation but the HGHG harmonic would.

CONCLUSION

EEHG is a new technique that not many facilities will be equipped to attempt in the near future. It can be partially attributed to luck that the ORS-sFLASH section is so ideally suited to do EEHG experiments. The last 3 months of 2011 will provide an ideal opportunity to upgrade the first ORS chicane and install a new laser transport line which will make this experiment possible. It will provide for new uses of the sFLASH infrastructure and diagnostics as well as significant contributions from non-DESY personnel. It will not impact any existing FLASH experiments and it will provide valuable experience for FLASH II planning. A first look has been given to issues surrounding CSR, LSC-microbunching, magnet tolerance, and general experiment design and optimization.

ACKNOWLEDGEMENTS

Thank you to Atoosa Mesek (HZB) for suggesting useful initial references and to Velizar Miltchev for GENESIS files and instruction for the sFLASH undulator section. The research work was supported by DESY and BMBF grant 05K10PE1.

REFERENCES

[1] D. Xiang and Stupakov, *Echo-enabled Harmonic Generation for Free Electron Lasers*, SLAC-PUB-13474, Dec 2008.

[2] G. Stupakov, *Using the Beam-Echo Effect for Generation of Short Wavelength Radiation*, PRL.102.074801 2009.

[3] D. Xiang and G. Stupakov, *Tolerance study for the echo-enabled harmonic generation free electron laser*, SLAC-PUB-13644, May 2009.

[4] G. Stupakov, Invited Talk on EEHG, 2010 International Particle Accelerator Conference in Kyoto, Japan, May 2010.

[5] E. Allaria, et al., *Echo Enhanced Harmonic Emission in FERMI*, Proc. of FEL'09 (Liverpool).

[6] S. Reiche, et al. *Echo Enabled Harmonic Generation Scheme for SWISSFEL*, Proc. of FEL'09 (Liverpool).

[7] H. Deng, et al., *The Echo-Enabled Harmonic Generation (EEHG) Options for FLASHII*, FLASH Seminar December 06, 2010.

[8] D. Xiang et al., *Demonstration of the Echo-Enabled Harmonic Generation Technique for Short-Wavelength Seeded Free Electron Lasers*, PRL, 105, 114801 (2010).

[9] Z. T. Zhao et al., *Progress in SDUV-FEL and Development of X-Ray FELs in Shanghai*, proceedings of the 2010 Proc. of FEL'10 (Malmoe).

[10] K. Hacker, et al., *New Uses for the ORS Section at FLASH*, TESLA-FEL 2011-03.

[11] K. Hacker, *Requirements for Parasitic Operation of the ORS Section*, TESLA-FEL 2011-04.

[12] K. Hacker, et al., *Progress towards Echo-Seeding at FLASH in 2012*, TESLA-FEL 2011-06.

[13] Ya, S, Derbenev, et al. *Microbunch Radiative Head-Tail Interaction*, TESLA-FEL 1995-05.

[14] A.W. Chao and M. Tigner, *Handbook of Accelerator Physics and Engineering* (World Scientific, Singapore, 2006), 3rd ed.

[15] S. Reiche, Nuclear Instruments and Methods A429 (1999) p. 243.

[16] S. Reiche, Invited-talk, Proc. of FEL'11 (Shanghai).

[17] C. Behrens, DESY-thesis (to-be-published).

[18] R. Tarkeshian, et al., *Femtosecond Resolved Determination of Electron Beam and XUV Seed Pulse Temporal Overlap in sFLASH*, Proc of PAC'11 (New York).

[19] E.L. Saldin, et al., *Study of a noise degradation of amplification process in a multistage HGHG FEL*, Optics Communications 202 (2002) 167-187.

[20] E. Schneidmiller and M. Yurkov, Beam Dynamics Meeting, 8 March 2010.

[21] B. Schmidt et al., *Coherent Micro-bunching Radiation from Electron Bunches at FLASH in the 10 Micrometer Wavelength Range*, Proc. of FEL'08 (Gyeongju).
[22] S. Wesch et al. *Observation of Coherent Optical Transition Radiation and Evidence for Microbunching in Magnetic Chicanes*, Proc. of FEL'09 (Liverpool).
[23] E. Schneidmiller & M. Yurkov, Beam Dynamics Seminar, 8 March 2010.
[24] Saldin, Schneidmiller, Yurkov, TESLA-FEL-NOTE-2003-02.
[25] B. Schmidt, Workshop on the Microbunching Instability III, Frascati, 25 March 2010.
[26] S. Wesch, personal communication.
[27] P. Schmueser, et al., "Ultraviolet and Soft X-Ray Free-electron Lasers," Springer p.14-16 (2008).
[28] Z. Huang et al., *Measurements of the linac coherent light source laser heater and its impact on the x-ray free-electron laser performance*, PRST-AB 13(2010)020703.
[29] J. Rossbach, et al., *Erzeugung sehr kurzer, kohaerenter Strahlungspulse mittels High Harmonic Seeding bei FLASH*, Antrag 26, Feb 2010.
[30] L. Giannessi et al., *Implementing a HHG-Laser as seed in a HGHG-FEL*, EUROFEL-Report-2007-DS4-098.
[31] I. Ben-Zvi, K.M. Lang, L.H. Yu, Nucl. Instrum. and Meth. A 318, p. 726-729 (1992).
[32] R. Bonifacio, et al., Nucl. Instrum. and Meth. A 296, p. 358 (1990).
[33] T. Watanabe, et al., *Experimental characterization of superradiance in a single-pass high-gain laser-seeded free-electron laser*, Phys. Rev. Lett. 98, 038402 (2007).
[34] H. Wiedemann, Particle Accelerator Physics II, 2nd ed. Springer, Berlin Heidelberg 1999.
[35] L. Giannessi, personal communication.
[36] L. Giannessi, *Harmonic Generation and Linewidth Narrowing in Seeded FELs*, Proc. of FEL'04.